Available online at www.most.gov.bd
Volume 05, Page: 83-92, 2023
DOI: https://doi.org/10.3329/jscitr.v5i1.74008

Ministry of Science and Technology
Government of the People's of Bangladesh
Bangladesh Secretariat, Dhaka

Performances of MnO_2 and SnO_2 Coated MnO_2 as Cathode Materials for Aqueous Rechargeable Zinc-ion Batteries

Parbhej Ahamed[1]*, Md. Ibrahim Hossain Mollah[1], Md. Saddam Hossain[1], Rabeya Sultana Mim[1], Rakhi Kundu[1], Nishat Mahal Ira[1], Nusrat Tazeen Tonu[1], Md. Mahfujul, Hasan[2] and Mohammad Abu Yousuf[1*]

[1]*Department of Chemistry, Khulna University of Engineering & Technology, Khulna-9203*
[2]*Institute of Food Science & amp; Technology, Bangladesh Council of Scientific and Industrial Research, Dhanmondi, Dhaka-1205, Bangladesh*

Received:05.05.2023
Revised: 12.12.2023
Accepted: 12.052024

Abstract

In this study, the micro-emulsion method was used to create the manganese-based cathode materials MnO_2 and MnO_2@SnO_2. For the use as cathode materials in rechargeable zinc-ion batteries, MnO_2 and SnO_2 coated MnO_2@SnO_2 were synthesized. FT-IR, Powder X-ray Diffraction (XRD), Field Emission Scanning Electron Microscopy (FESEM), Energy Dispersive X-ray Spectroscopy (EDS), and UV-visible Spectroscopy were used to characterize the as-prepared materials. Electrochemical impedance spectroscopy (EIS), battery charge-discharge (BCD), and cyclic voltammetry (CV) techniques were used to investigate the electrochemical properties of the prepared cathode materials for aqueous rechargeable zinc-ion batteries (ARZIBs). The CV profiles were measured in the potential range of 2.1-1.0 V at a scan rate of 20 mV/s. A pair of redox peaks can be seen in the cycle of CV curves. Charge/discharge cycles of SnO_2 coated MnO_2@SnO_2 electrodes are higher than those of pristine MnO_2. SnO_2 coated MnO_2@SnO_2 electrodes have better initial charge/discharge capacities than pristine MnO_2 electrodes, which is a factor to take into account. In the first cycle, SnO_2 coated MnO_2@SnO_2 electrode has a 26% higher charge capacity than the bare MnO_2 electrode. The SnO_2 coating on MnO_2 may be the cause of the enhanced charge and discharge capabilities of MnO_2@SnO_2.

Keywords: Micro-emulsion method, SnO_2 coated manganese dioxide, Aqueous rechargeable zinc-ion battery

Introduction

Quality aspects of humanitarian need and economical activities of a country are directly dependent upon the amount of energy consumption [Lambert *et al*., 2014]. Energy is considered a basis input commodity to shape various important world issues such as international relation and economy. In today's world, energy resources is thereby regarded as a strategic scale for the level of economic development of a country. They push the existing techno-sphere of today's society into a new tomorrow's one. Accordingly, the advent of rechargeable battery technologies as energy storage resources have been attracted much more attention because of their convenience and stability during utilization [Larcher and Tarascon 2015]. So far, various rechargeable batteries (Li^+, Na^+, K^+, Ca^{2+}, Zn^{2+}, Al^{3+}) in aqueous and non-aqueous system have been developed [Su *et al*., 2017; Suo *et al*., 2017 & Xia et. at., 2018]. Among the developed aqueous rechargeable zinc-ion batteries (ARZIBs) have achieved the global limelight newly as next generation safe energy storage device due to their environmental benignity, abundant resources, low cost, reliable safety and

*Corresponding author e-mail: parbhej@chem.kuet.ac.bd

affordability [Wang *et al*., 2021]. They have been considered as promising and potential candidate to substitute non-aqueous rechargeable batteries. In a typical ARZIBs Zn^{2+} from zinc metal anode reversibly intercalated into the host cathode structure in aqueous zinc containing electrolyte environment. Many studies have been thereby applied to manganese based oxides (Mn_xO_y), vanadium based oxides (V_xO_y), Prussian blue analogues and some organic polymers based materials to find the suitable host for ARZIBs [Li *et al*., 2020]. Among them MnO_2 polymorphs with tunnel, layer and spinel based architecture have attracted great attention for the advancement of ARZIBs owing to high theoretical capacity (308 mA h g^{-1}), cost effectiveness and low toxicity. However, the development of rechargeable Zn || MnO_2 system are dramatically limited due to severe phase transition behavior of MnO_2 host during charge/discharge processes.

Manganese dissolution and hydrated Zn^{2+} ions insertion are mainly responsible for severe structural transition of MnO_2. These drastic phase transition behavior of MnO_2 induces large volumetric transformation, creates collapsed structure and independent of the original architecture [Le *et al.*, 2021]. As a result, cyclic performance and capacity of aqueous Zn || MnO_2 system significantly reduce and hindere their practical applications. This puzzling structural phenomenon has motivated battery researchers for designing suitable architecture MnO_2 material for the development of aqueous rechargeable Zn || MnO_2 battery. There are no reports of stable cycling of MnO_2 cathode materials for ARZIBs. But there are some reports about the cycle life of MnO_2 in aqueous mild electrolyte system. Among them Liu's *et al.* reported 45 cycles of MnO_2 cycle life and found maximum 260 mAh/g specific capacity [Guo *et al*., 2020]. Alongside, Chen *et al*. has demonstrated 230 mAh/g specific capacity MnO_2 cathode in 150 cycles [Guo *et al*., 2019]. Thus, the development of structurally stable MnO_2 materials for long cycle life Zn || MnO_2 system are still posing a great challenge to the battery researchers. These challenges are still need to be overcome for designing ARZIBs with outstanding electrochemical battery performance. As mentioned above, the poor cycling performance of MnO_2 materials are mainly due to the contribution from the structure transformation of MnO_2 and hydrated Zn^{2+} ions insertion into MnO_2 structure. A promising solution to address this problem is to strengthen the structure of MnO_2 via coating with metal oxides. Henceforth, it has been planned to investigate the influence of SnO_2 coating on MnO_2 cathode materials for energy storage performance in ARZIBs. Greater initial charge/discharge capacities are exhibited by SnO_2-coated MnO_2@SnO_2 electrodes compared to pure MnO_2 electrodes.

Materials and Methods

The methodology of the proposed project consists of four parts. First part is the preparation of MnO_2 and MnO_2@SnO_2 (5 wt% of SnO_2 to MnO_2) electrode material using water in oil micro-emulsion technique (Figure 1). The second part consists of the physical characterization of the prepared MnO_2@SnO_2 electrode materials using various techniques. Next part is the fabrication of CR-2032 coil cell. The final part is to investigate the electrochemical performance of the fabricated CR-2032 coil cell.

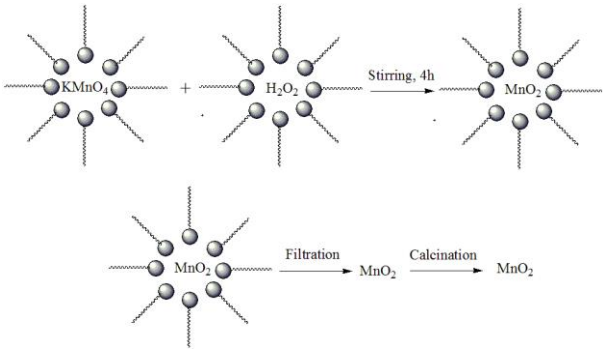

Figure 1. Schematic illustration of the preparation of MnO_2 nano-materials.

Synthesis of SnO_2 Coated Manganese Oxide

Cyclohexane, Triton X-100 and cyclohexanol used as oil phase, surfactant and co-surfactant, respectively, for the preparation of micro-emulsion. The desired amount of cyclohexane, Triton X-100 and cyclohexanol taken in two separate beaker with 5:3:2 volume ratios and

then magnetically stirred. Aqueous solution of potassium permanganate ($KMnO_4$) and hydrogen peroxide (H_2O_2) were added dropwise to a beaker to prepare one micro-emulsion (ME1). Another two micro-emulsions were prepared by adding stoichiometric amount of stannous chloride and sodium hydroxide to two separate beakers. Stannous chloride and sodium hydroxide containing beakers are termed ME2 and ME3, respectively. ME1 was stirred for a certain period of time to form manganese dioxide (MnO_2). Then, ME2 was added dropwise to ME1 and stirred for another 30 mins. Afterwards, ME3 was added to the solution for the formation of MnO_2@$Sn(OH)_2$. Calcination of MnO_2@$Sn(OH)_2$ at 300 ^oC in open atmospheric condition resulted MnO_2@SnO_2.

Fabrication of CR-2032 Coin Cell

CR-2032 cell was fabricated as coin cell. The cathode electrode was prepared by mixing MnO_2@SnO_2, carbon black (C) and poly(vinylidene fluoride) (PVDF) at the weight ratio of 8:1:1. N-methyl pyrolidone used to prepare the slurry of the mixture. The prepared slurry was coated on stainless steel plate and dried at 80 ^oC. Zinc sulphate ($ZnSO_4$) used as electrolyte. Filter paper was used as separator. Zinc foil was used as anode. Along with them other components like spacer, ring and case were used to fabricate CR-2032 coin cell.

Results and Discussion

Using the straightforward micro-emulsion technique, MnO_2 and 5% SnO_2 coated MnO_2@$SnO_2$was produced (MnO_2). The produced MnO_2 and MnO_2@SnO_2 materials were characterized using UV-visible spectroscopy, FT-IR, FESEM, XRD and EDS techniques. The produced MnO_2 and MnO_2@SnO_2 were utilized to construct the CR-2032 coin cell, and the cell was then electrochemically assessed.

UV-Vis Spectroscopic Analysis

Utilizing UV-Vis methods, the band gap energy of the produced MnO_2 nanoparticles was examined. Figure 2 depicts the spectrum obtained from the produced MnO_2 and SnO_2 coated MnO_2@SnO_2. The UV-Visible reflectance spectra of the manufactured materials were used to calculate the optical band gap energy (E_g) of the materials using the Tauc method. The typical reflectance spectra of MnO_2 and MnO_2@SnO_2 are shown in Figures 2 (a) and 2 (c) respectively. Figures 2 (b) and 2 (d) display the calculated band gap energies of MnO_2 and MnO_2@SnO_2 using the derivation of absorption spectrum fitting method. According to the graph, the band gap energies of MnO_2 and MnO_2@SnO_2 are, respectively, 3.2 and 3.1 eV. This suggests that the SnO_2 coated MnO_2 has a red-shift of 0.1 eV relative to the pristine MnO_2 alone. The reason for this reduction in band gap is the SnO_2 coating on the MnO_2 surface.

FTIR Analysis

FTIR analysis was used to identify the presence of key functional groups in MnO_2 and MnO_2@SnO_2. Figure 3 shows the observed FTIR spectra of MnO_2 and MnO_2@SnO_2. The absorption bands in this IR spectra typically range from 400–4000 cm^{-1}, with 527, 722 and 1380 cm^{-1} being the most common. The Mn-O stretching mode of MnO_2 is revealed by the absorption band at 527 cm^{-1}, which indicates the presence of a Mn-O bond inside the MnO_2 structure [Bin et al., 2018 and Chao *et al*., 2018]. Peak at 527 cm^{-1} for MnO_2@SnO_2 has been broadened by the stretching modes of both Sn-O-Sn and Mn-O. The band for MnO_2@SnO_2 widened at 527 cm^{-1}, indicating that SnO_2 was successfully coated on the MnO_2 surface. The O-H bending vibrations paired with Mn atoms are responsible for the bands that exist between 720 and 1380 cm^{-1} Kundu *et al.*, 2016). In the MnO_2 and MnO_2@SnO_2 structures, the existence of absorbed water molecules is attributed to the usual broad absorption in the wavelength ranges of 3200 and 3600 cm^{-1}. The band at 1616 cm^{-1}, on the other hand, represented the bending collision of adsorbed water. Both of these bands were present at the same time, indicating the presence of an adsorbed H_2O molecule in this sample (Wei et al., 2012 and Xu et al., 2012].

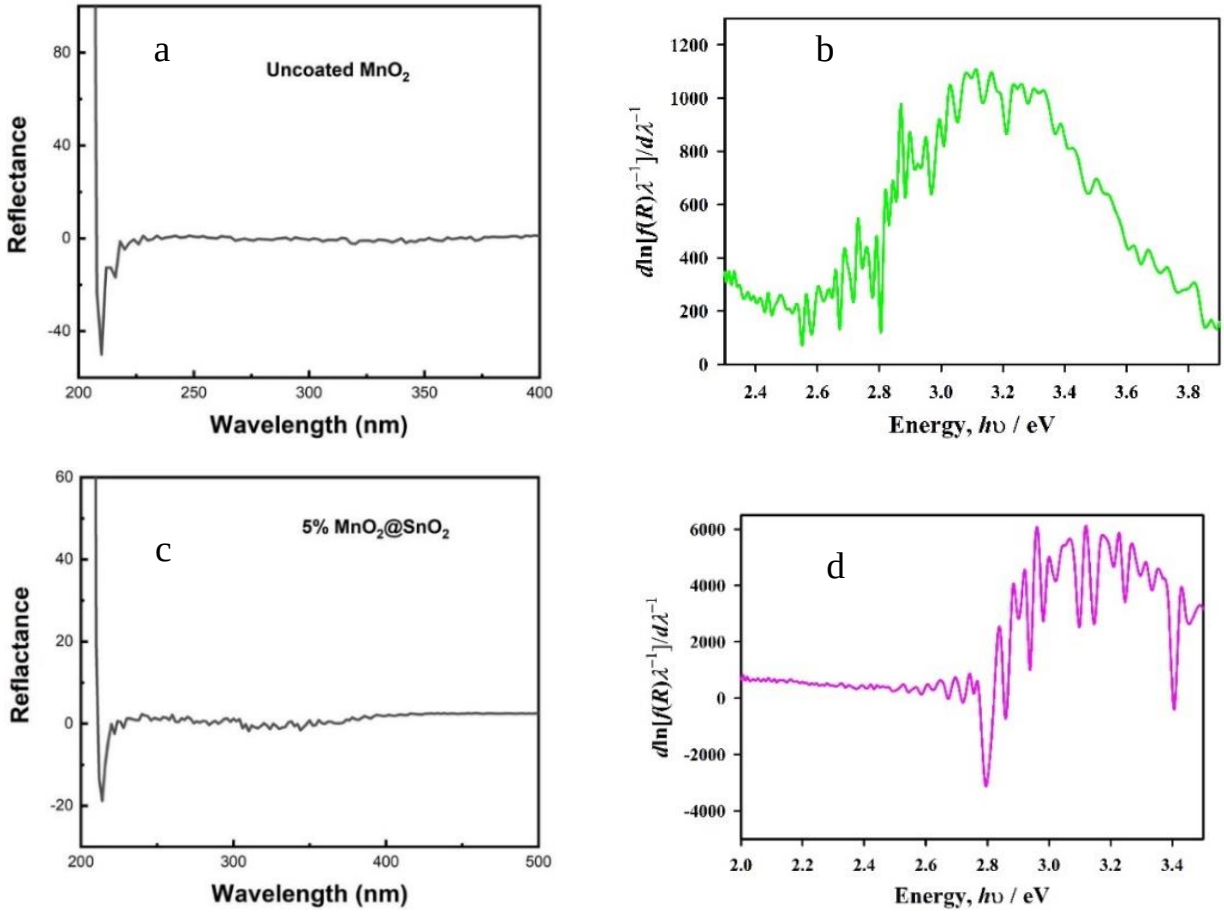

Figure 2. Typical reflectance spectrum of (a) MnO_2 and (c) MnO_2@SnO_2. Estimation of E_g according to derivation of absorption spectrum fitting method of (b) MnO_2 and (d) MnO_2@SnO_2.

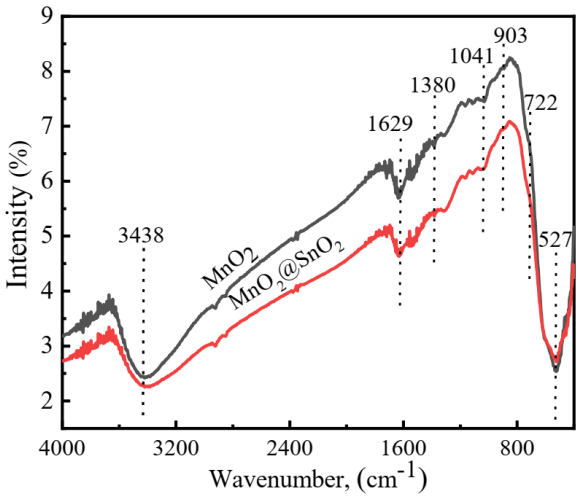

Figure 3. FTIR spectrum shown by the prepared sample.

XRD Analysis

X-ray diffraction patterns validated the phase purity and crystalline nature of the prepared MnO_2 and MnO_2@SnO_2 samples. The prepared sample's X-ray diffraction pattern is shown in the Figure 4. The production of α-MnO_2 is indexed by XRD patterns with diffraction peaks at 12.7, 18.1, 28.8, 37.5, 42.1, 49.9, 56.2, and 60.3° (2θ). The (110), (200), (310), (211), (301), (411), (600) and (521) planes are represented by the peaks. Peak positions at 28 and 37° of 2θ can be ascribed to the formation of a SnO_2 layer on the MnO_2 surface. Hence, all of the diffraction peaks are well correlated with MnO_2 and SnO_2 published values in the literature [Alfaruqi et al., 2017 and Lu *et al*., 2017]. There are no impurity peaks that could be identified. According to the XRD data, the as-prepared materials are pure phase MnO_2 and MnO_2@SnO_2.

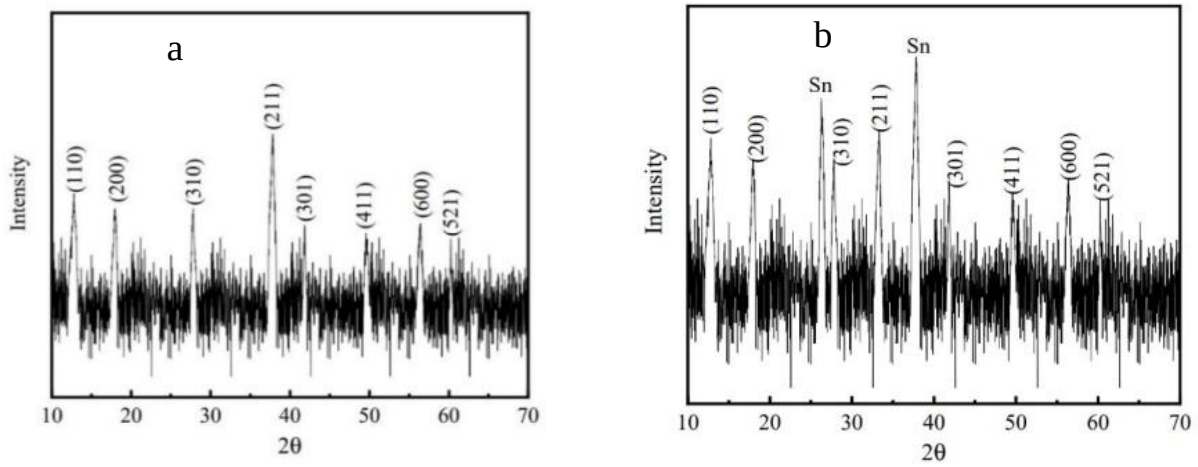

Figure 4. XRD patterns of the prepared samples (a) MnO_2 and (b) MnO_2@SnO_2

FESEM Analysis

The morphology of the produced MnO_2 and MnO_2@SnO_2 materials was determined using fFESEM. Figure 5 depicts the shape of the prepared MnO_2 materials. Figure 5 (b) shows the histogram that corresponds to Figure 5 (a). Figure 5 (c) illustrate morphology of MnO_2@SnO_2 materials. The histograms of Figure 5 (c) is shown in Figures 5 (d). As shown in Figure 5 (a) and Figure5 (c), it can be concluded that the particles of MnO_2 and MnO_2@SnO_2 are compactly packed and practically spherical in shape. As an irregular structure of agglomeration, the spherical form of MnO_2 and MnO_2@SnO_2 have been observed. The aggregation of prepared MnO_2 and MnO_2@SnO_2 materials may be affected by crystal face attraction interactions, van der Waals forces, hydrogen bonding, and hydrophobic interactions on MnO_2 and MnO_2@SnO_2 nanoparticle surfaces may also be responsible for the aforementioned interaction, in addition to crystal face attraction. The synthesized MnO_2 and MnO_2@SnO_2 have average particle sizes of 20 nm and 45 nm, as seen in the histogram.

EDS Analysis

The elemental composition of the generated MnO_2 and MnO_2@SnO_2 nanoparticles was determined using EDSinvestigations. The elemental analysis of MnO_2 and MnO_2@SnO_2 nanoparticles are shown in Figure 6. Elemental analytical data, which shows a very high signal for Mn and O, confirms the presence of MnO_2 in the manufactured MnO_2 and MnO_2@SnO_2 materials. In the EDS spectrum of Figure 6 (b) the element Sn has been found. Apart from Mn and O, the elemental analysis data also shows traces of K and C. Remains of K could be the result from the reactions mixture. The carbon tap of the sample holder is responsible for the C signal in this image.

Electrochemical Characterization

The electrochemical performance of the produced samples MnO_2 and MnO_2@SnO was tested using coin cells. The synthesized cathode material was used to build and test the CR-2032 coin cells. This section delves deeper into the details of a number of electrochemical characterizations.

Cyclic Voltammetry

Figure 7 shows the CV profiles of Zn-MnO_2 and Zn-MnO_2@SnO_2 cell in an aqueous electrolyte of 2.0 M $ZnSO_4$ to investigate the electrochemical parameters of the manufactured battery. The CV profiles were recorded at a scan rate 20 mV/s in the potential range 2.1–1.0 V. A pair of redox peaks can be seen in the cycle of CV curves. Zn^{2+} de-intercalation from Zn foil, occurs around 1.62 V in the anode scan. The oxidation of Zn metal to Zn^{2+} and intercalation into the tunnel structure of MnO_2 are both involved in this process. The transition of MnO_2 to $ZnMnO_2$ is related with Zn^{2+} intercalation into the tunnel structure of MnO_2. Meanwhile, a reversible peak appeared at ~1.32 V in the cathode scan. Zn^{2+} de-intercalates from $ZnMnO_2$ in the reversible process and MnO_2 returns to its original tunnel structure.

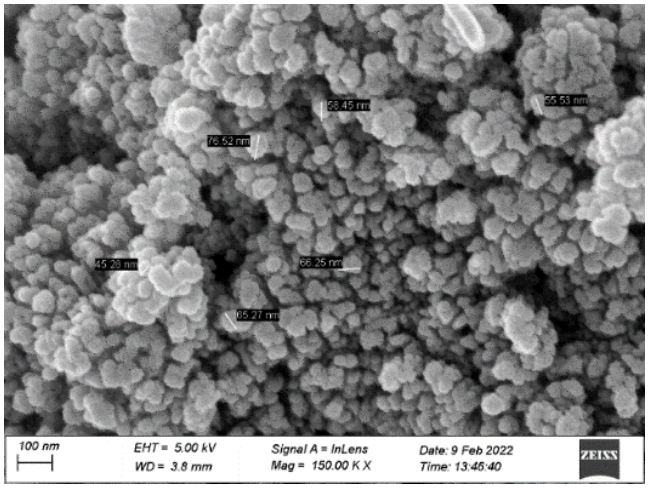

(a) FESEM images of uncoated MnO_2

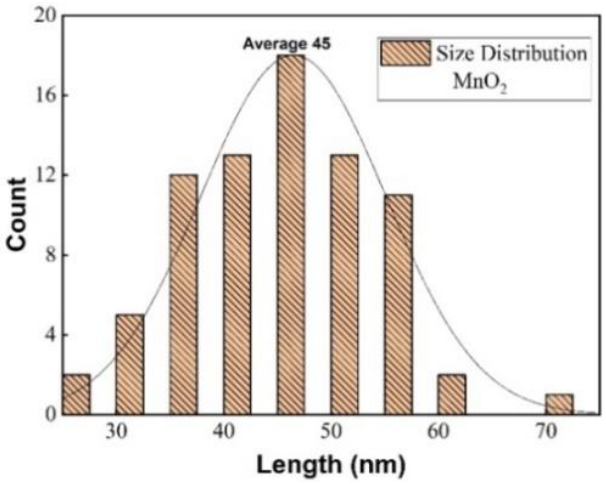

(b) Histogram of image (a)

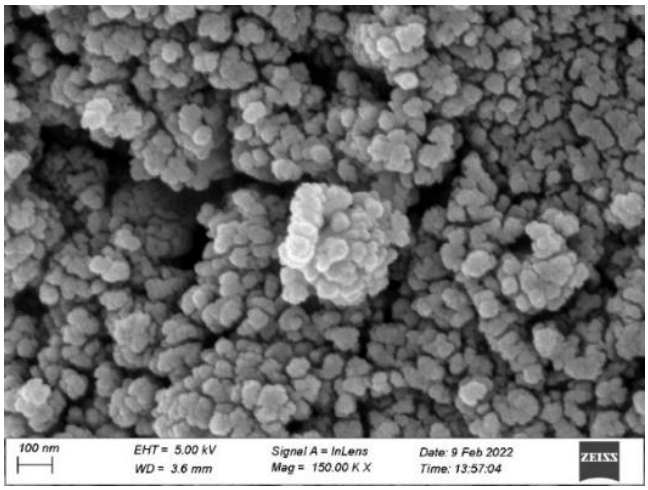

(d) Histogram of image (c)

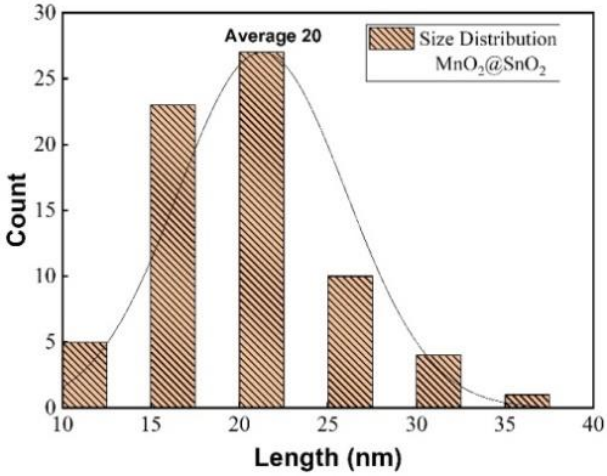

(c) FESEM images of of MnO_2@SnO_2

Figure 5. FESEM images and corresponding histogram of the prepared MnO_2 and MnO_2@SnO_2 materials.

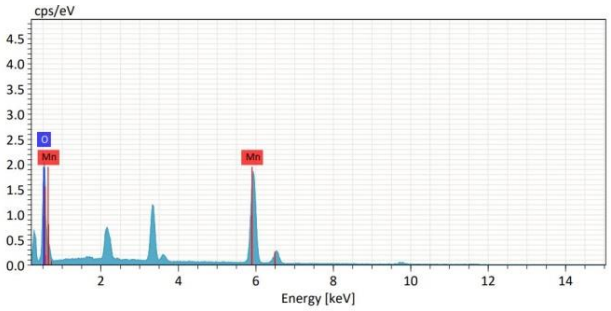

(a)

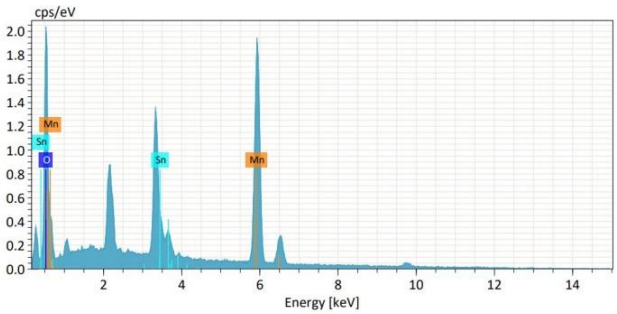

(b)

Figure 6. EDS pattern of the prepared (a) MnO_2 (b) MnO_2@SnO_2.

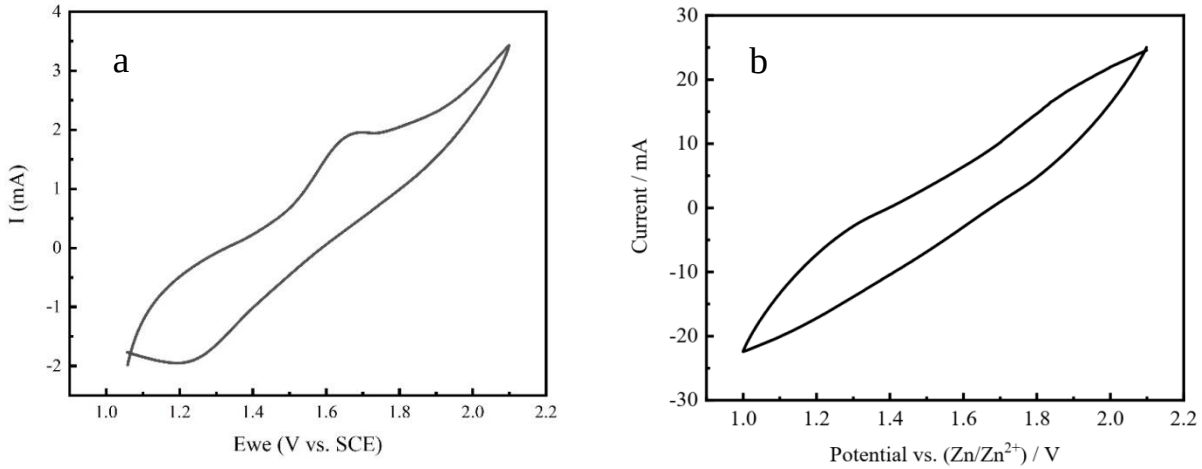

Figure 7. Cyclic voltammograms of the coin cell using (a) MnO_2 (b) MnO_2@SnO_2.

The CV profiles of the pristine MnO_2 electrode differ slightly from those of the SnO_2 coated MnO_2@SnO_2 electrode. Nonetheless, all of the constructed electrode's CV cycles are identical in shape and appear to coincide. Hence, anode and cathode peaks observation in both Zn/MnO_2 and Zn/MnO_2@SnO_2 cells, indicating their redox behavior. The following reactions are linked with the intercalation and de-intercalation processes of Zn^{2+} ion into MnO_2 and MnO_2@SnO in the cathode and anode scans.

De-intercalation reaction : Zn foil=Zn^{2+} + $2e^-$ (1)

Intercalation reaction : MnO_2 + Zn^{2+} + $2e^-$ = $ZnMnO_2$ (2)

Overall cell reaction : Zn + MnO_2 = $ZnMnO_2$ (3)

Battery Charge Discharge

Figure 8 shows the charge/discharge curves of MnO_2 and MnO_2@SnO at 1 mA. The observed CV curves in Figure 7 are consistent with charge/discharge plateaus around 1.6 and 1.3 V. Charge/discharge cycles of SnO_2 coated MnO_2@SnO_2 electrodes are higher than those of bare MnO_2. The factor to consider is that SnO_2 coated MnO_2@SnO_2 electrodes have higher initial charge/discharge capabilities than bare MnO_2 electrodes. When compared to a MnO_2@SnO_2 electrode, the charge capacity value has increased by 3%. The increased charge and discharge capabilities of MnO_2@SnO_2 may be due to the SnO_2 coating on MnO_2.

Comparison of Cycle Number of MnO_2 and MnO_2@SnO_2

The capacity of MnO_2 electrode batteries has been found to be essentially stable up to 10 cycles. The battery can be cycled up to 14 times with MnO_2@SnO_2 electrode. The cathodes MnO_2 and MnO_2@SnO_2 may thus retain reversible and nearly stable capacities up to the aforementioned cycles at 1 mA applied current. Following that, the electrodes may experience severe Zn^{2+} dissolving in electrolyte, causing the capacity to become unstable.

Electrochemical Impedance Spectroscopy of prepared MnO_2 and SnO_2 coated MnO_2@SnO_2

The EIS spectra of the as-prepared MnO_2 and MnO_2@SnO_2 electrodes are in the 10–100 kHz frequency range (vs. SCE) and have a 5 mV amplitude (Figure 9). High-frequency semicircles and a low-frequency oblique line appeared in the Nyquist plots. The ohmic resistance (R_s), which includes the electrode intrinsic resistance as well as the ion/electron resistances through the electrolyte, separator, and SEI film, is represented by the intercept on the real axis. The high-frequency semicircle diameter of the MnO_2@SnO_2 sample is significantly smaller than that of the other electrodes, according to the photographs of the high-frequency region of all the samples. The MnO_2@SnO sample with SnO_2 coating had the lowest R_s value, indicating improved charge transfer between the electrolyte and electrode.

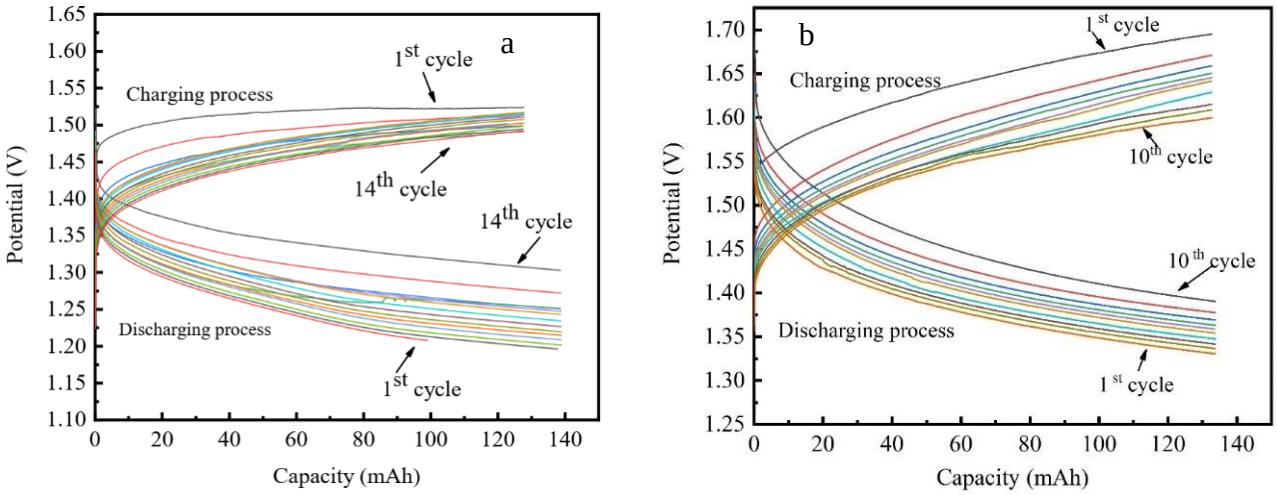

Figure 8. BCD cycles of the fabricated coin cell using (a) MnO_2 (b) MnO_2@SnO_2 cathode.

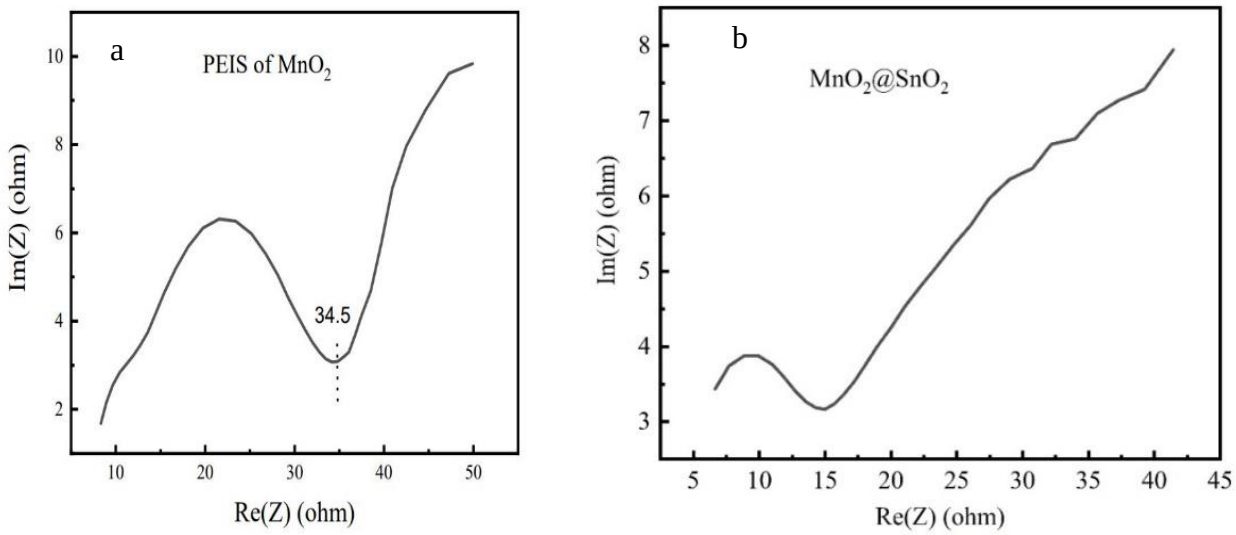

Figure 9. EIS data of the fabricated coin cell before BCD using (a) MnO_2 and (b) MnO_2@SnO_2 cathode.

Conclusions

In conclusion, MnO_2@SnO_2 composite was successfully produced in this study using the simple sol-gel approach and then utilized as an aqueous ZIBs cathode. A lower band gap value and increased structural stability are the results of SnO_2 anchoring on MnO_2. The reversible capacity of the MnO_2@SnO_2 combination is greater than that of pure MnO_2. The findings could open a path for the development of ZIB cathode materials.

Acknowledgements

This research was done by the financial support of Ministry of Science and Technology (Fiscal Year 2021-2022).

Declaration

The authors declare that this research findings reported in this article do not have any conflicting interest.

Author's contribution

Parbhej Ahamed & Md. Ibrahim Hossain Mollah: Methodology, Investigation, Formal Analysis, Writing -

Original Draft ; Md. Saddam Hossain, Md. Mahfujul Hasan, *Nishat Mahal Ira & Md. Ibrahim Mollah*: Analysis, Validation, Review & Editing; *Mim & Nusrat Tazeen Tonu:* Resources, Writing - Review & Editing, Project administration; *Parbhej Ahamed & Mohammad Abu Yousuf*: Conceptualization, Resources, Writing-Review & Editing, Funding acquisition, Visualization, Supervision.

References

Alfaruqi MH, Mathew V, Song J, Kim S, Islam S, Pham DT, & Kim J (2017), Electrochemical zinc intercalation in lithium vanadium oxide: a high-capacity zinc-ion battery cathode. *Chemistry of Materials*, **29(4)**, 1684-1694.

Bin D, Wang F, Tamirat AG, Suo L, Wang Y, Wang C, & Xia Y (2018), Progress in aqueous rechargeable sodium-ion batteries. *Advanced Energy Materials*, **8(17)**, 1703008.

Chao D, Zhu C, Song M, Liang P, Zhang X, Tiep NH, & Fan HJ, (2018), A high-rate and stable quasi-solid-state zinc-ion battery with novel 2D layered zinc orthovanadate array. *Advanced Materials*, **30(32)**, 1803181.

Guo C, Tian S, Chen B, Liu H, & Li J (2020), Constructing α-MnO_2@ PPy core-shell nanorods towards enhancing electrochemical behaviors in aqueous zinc ion battery. *Materials Letters*, **262**, 127180.

Guo C, Zhou Q, Liu H, Tian S, Chen B, Zhao J, & Li J (2019), A case study of β-and δ-MnO_2 with different crystallographic forms on ion-storage in rechargeable aqueous zinc ion battery. *Electrochimica Acta*, **324**, 134867.

Kundu D, Adams BD, Duffort V, Vajargah SH, & Nazar LF (2016), A high-capacity and long-life aqueous rechargeable zinc battery using a metal oxide intercalation cathode. *Nature Energy*, **1(10)**, 1-8.

Lambert JG, Hall CA, Balogh S, Gupta A, & Arnold M (2014), Energy, EROI and quality of life. *Energy policy*, **64**, 153-167.

Larcher D, & Tarascon JM (2015), Towards greener and more sustainable batteries for electrical energy storage. *Nature Chemistry*, **7(1)**, 19-29.

Le T, Sadique N, Housel LM, Poyraz AS, Takeuchi ES, Takeuchi KJ, & Liu P (2021), Discharging behavior of hollandite α-MnO_2 in a hydrated zinc-ion battery. *ACS applied materials & interfaces*, **13(50)**, 59937-59949.

Li C, Zhang X, He W, Xu G, & Sun R (2020), Cathode materials for rechargeable zinc-ion batteries: From synthesis to mechanism and applications. *Journal of Power Sources*, **449**, 227596.

Lu K, Song B, Zhang Y, Ma H, & Zhang J (2017), Encapsulation of zinc hexacyanoferrate nanocubes with manganese oxide nanosheets for high-performance rechargeable zinc ion batteries. *Journal of Materials Chemistry A*, **5(45)**, 23628-23633.

Su D, McDonagh A, Qiao,SZ, & Wang G (2017), High-capacity aqueous potassium-ion batteries for large-scale energy storage. *Advanced Materials*, **29(1)**, 1604007.

Suo L. Borodin O, Wang Y, Rong X, Sun W, Fan X, & Wang C (2017), "Water-in-salt" electrolyte makes aqueous sodium-ion battery safe, green, and long-lasting. *Advanced Energy Materials*, **7(21)**, 1701189.

Wang X, Zhang Z, Xi B, Chen W, Jia Y, Feng J, & Xiong S (2021), Advances and perspectives of cathode storage chemistry in aqueous zinc-ion batteries. *ACS nano*, **15(6)**, 9244-9272.

Wei C, Xu C, Li B, Du H, & Kang F (2012), Preparation and characterization of manganese dioxides with nano-sized tunnel structures for zinc ion storage. *Journal of Physics and Chemistry of Solids*, **73(12)**, 1487-1491.

Xia C, Guo J, Lei Y, Liang H, Zhao C, & Alshareef HN (2018), Rechargeable aqueous zinc-ion battery based on porous framework zinc pyrovanadate intercalation cathode. *Advanced Materials*, **30(5)**, 1705580.

Xu C, Li B, Du H, & Kang F, (2012), Energetic zinc ion chemistry: the rechargeable zinc ion battery. *Angewandte Chemie*, **124(4)**, 957-959.